

# Conductivity of Langmuir-Blodgett films of a disk-shaped liquid-crystalline molecule–DNA complex studied by current-sensing atomic force microscopy

Alpana Nayak<sup>1</sup> and K. A. Suresh<sup>2,\*</sup><sup>1</sup>*Raman Research Institute, Sadashivanagar, Bangalore 560 080, India*<sup>2</sup>*Centre for Liquid Crystal Research, P.B. No. 1329, Jalahalli, Bangalore 560 013, India*

(Received 4 April 2008; revised manuscript received 6 June 2008; published 27 August 2008)

We have studied the electrical conductivity in monolayer films of an ionic disk-shaped liquid-crystal molecule, pyridinium tethered with hexaalkoxytriphenylene (PyTp), and its complex with DNA by current-sensing atomic force microscopy (CS-AFM). The pure PyTp and PyTp-DNA complex monolayer films were first formed at the air-water interface and then transferred onto conducting substrates by the Langmuir-Blodgett (LB) technique to study the nanoscale electron transport through these films. The conductive tip of CS-AFM, the LB film, and the metal substrate form a nanoscopic metal-LB film-metal (*M-LB-M*) junction. We have measured the current-voltage (*I-V*) characteristics for the *M-LB-M* junction using CS-AFM and have analyzed the data quantitatively. We find that the *I-V* curves fit well to the Fowler-Nordheim (FN) model, suggesting electron tunneling to be a possible mechanism for electron transport in our system. Further, analysis of the *I-V* curves based on the FN model yields the barrier heights of PyTp-DNA complex and pure PyTp films. Electron transport studies of films of ionic disk-shaped liquid-crystal molecules and their complex with DNA are important from the point of view of their applications in organic electronics.

DOI: [10.1103/PhysRevE.78.021606](https://doi.org/10.1103/PhysRevE.78.021606)

PACS number(s): 68.47.Pe, 68.37.Ps, 73.40.Rw, 61.30.-v

## I. INTRODUCTION

Disk-shaped liquid-crystal (DLC) molecules are promising materials for organic electronics. Their intrinsic electronic properties combined with their trend to form large ordered domains make them potential candidates for fabrication of devices like field-effect transistors, photovoltaic solar cells, and light-emitting diodes [1]. Compared to these conventional DLCs, ionic DLCs are significantly different due to the presence of ions as charge carriers [2]. Ionic DLCs find applications in designing anisotropic ion-conductive materials [3]. Moreover, cationic DLC molecules enlarge the scope for studying electrostatic interactions with negatively charged biological molecules like DNA [4,5]. The DNA molecule has drawn a lot of attention to nanoelectronic devices due to its intrinsic electronic properties [6]. The charge-transfer reactions and conductivity measurements show a large variety of possible electronic behavior, ranging from Anderson and band-gap insulators to effective molecular wires [7]. Since both DNA and DLCs have their own intrinsic electronic properties, complexing DNA with cationic DLC molecules is a novel approach for developing advanced materials with interesting electronic properties. For any such practical applications, it is necessary to have well-ordered thin films. Although there are several techniques to obtain thin films, the Langmuir-Blodgett (LB) technique is a convenient approach to obtain well-ordered films [8]. To study electron conduction at the molecular level, scanning probe techniques [scanning tunneling microscopy (STM) and current sensing atomic force microscopy (CS-AFM)] are the most suitable methods [9,10]. CS-AFM provides an attractive approach to electrically contacting monolayer films under controlled load and the formation of metal-molecule-metal junctions [11]. Additionally, in CS-AFM, the images of

topography and current are simultaneously obtained, enabling direct correlation of local topography with electrical properties at the nanoscale [12]. The conventional CS-AFM operates in contact mode. For soft systems, the damage due to lateral shear forces in contact-mode imaging is an important issue. Recently, Casuso *et al.* have introduced a methodology and performed the conductivity maps in jumping mode, rather than in contact mode, for biomembranes [13]. However, for systems like self-assembled monolayers and polymers, the contact mode can still be used [11,14].

We have formed films of an ionic disk-shaped liquid crystal, pyridinium tethered with hexaalkoxytriphenylene (PyTp), and its complex with DNA (PyTp-DNA) at the air-water interface. Using the LB technique, we have transferred the films onto solid substrates. We find that the formation of the DNA complex enhanced the transfer efficiency over several tens of layers. We believe that it is not only the ionic-ionic interaction, but the packing of the PyTp molecules and DNA molecules that brings the stability. This is indicated by the decrease in the limiting area and increase in surface pressure of the complex film as compared with the pure PyTp film [5]. LB film deposition is a physical adsorption process, and it is sensitive to the packing of molecules in a film and its stability [8]. The efficiency of the PyTp-DNA complex to form multilayers on a substrate can find applications in devices such as thin-film transistors and nucleic-acid-based biosensors [15,16].

In this article, we report electrical conductivity measurements at the nanoscale employing CS-AFM on monolayer films of PyTp and PyTp-DNA complex obtained by the LB technique. Our measurements show that the conductivity of the PyTp-DNA complex film is much less compared to the pure PyTp film. The ability to rationally design molecular electronic components hinges on a fundamental understanding of the charge transport mechanism in metal-molecule-metal junctions. To this end, we look for a possible mechanism for electron transport at the nanoscale in such a system.

\*Corresponding author. [suresh@clcr.res.in](mailto:suresh@clcr.res.in)

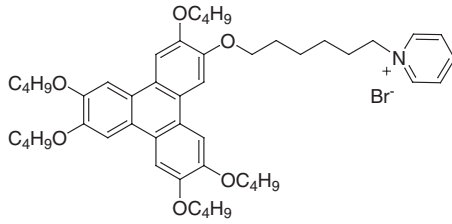


FIG. 1. Chemical structure of pyridinium tethered with hexaalkoxytriphenylene (PyTp) molecules.

The analysis of the current-voltage ( $I$ - $V$ ) curves suggests that the electron transport mechanism in our system follows the Fowler-Nordheim tunneling model.

## II. EXPERIMENT

The material PyTp (Fig. 1) was synthesized by Kumar and Pal [17]. It is a disk-shaped thermotropic liquid crystal. At room temperature, the material is in solid phase, and with an increase in temperature, it transforms to a columnar mesophase at 83.7 °C. Here, the PyTp disk-shaped molecules stack upon one another, giving rise to a columnar structure. On further increasing the temperature, the columnar mesophase transforms to isotropic liquid phase at 95 °C. On cooling, the columnar mesophase appears at 92 °C and remained stable down to room temperature. For its complexation with DNA, double-stranded deoxyribonucleic acid sodium salt from Salmon testes with an approximate molecular weight of  $1.3 \times 10^6$  and  $\sim 2000$  base pair was used (Sigma). The monolayer film of PyTp was prepared at the air-water ( $A$ - $W$ ) interface in a Langmuir-Blodgett trough (model 611M, NIMA). To obtain PyTp-DNA complex monolayer film at the  $A$ - $W$  interface, we used a  $10^{-8}$  M concentration of DNA in the ultrapure water subphase. The films were compressed to a target surface pressure of 35 mN/m, and then these films were transferred from the  $A$ - $W$  interface to solid substrates by the LB technique. We used two types of substrates for film deposition: gold-coated mica and polished doped silicon. The gold-coated mica substrates, which are hydrophilic, were obtained from Molecular Imaging. These substrates were very clean and hence just rinsed with HPLC-grade chloroform before film deposition. The silicon substrates were double-sided mirror polished, boron doped with resistivity  $\sim 0.0005 \Omega \text{ cm}$  and  $\langle 100 \rangle$  orientation, obtained from AppNano. To make the surface hydrophilic, the silicon substrates were dipped in hot piranha solution (mixture of concentrated  $\text{H}_2\text{SO}_4$  and  $\text{H}_2\text{O}_2$  in 3:1 ratio) for about 5 min and then rinsed thoroughly with ultrapure de-ionized water, before film deposition. Further details of film preparation are described elsewhere [5,18]. To determine the film thickness, we first scanned the film surface in tapping-mode AFM and obtained the topography image. Next, with the same tip, we scratched the film in contact mode and then imaged the scratched area in tapping mode. The height profile across the scratch on the film gave the film thickness. The conductivity measurements were carried out using a contact-mode CS-AFM (model PicoPlus, Molecular Imaging). We used platinum coated silicon cantilevers (probe model: ANSCM-PC,

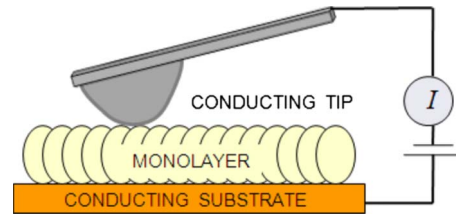


FIG. 2. (Color online) Schematic representation of a metal-molecule-metal junction formed by a conducting AFM tip in contact with a monolayer film deposited on a conducting substrate.

AppNano) having a spring constant in the range of 0.02–0.8 N/m, tip radius  $\sim 30$  nm, and resonance frequency in the range of 5–25 kHz for CS-AFM measurements. The conductive tip behaves effectively as a metal electrode with an area mainly determined by the tip-sample contact region. With the tip at virtual ground, a selectable bias voltage was applied between the tip and sample. A preamplifier, with a sensitivity of 1 nA/V and operational range from 1 pA to 10 nA, was used. In our CS-AFM apparatus, the rms noise level was about 2 pA and any signal above this value was detectable. The deflection of the cantilever was monitored and kept constant to maintain a constant force between the tip and sample, and simultaneous topographic and current images were generated. During  $I$ - $V$  measurements, the feedback loop was enabled, meaning that the force applied by the cantilever was held constant. All  $I$ - $V$  measurements were performed on gold substrates by placing the tip at the desired position on the film and carefully selecting the force. In addition, after every  $I$ - $V$  measurement, we scanned the same region of the film to ensure no damage.

An advantage of CS-AFM is its experimental simplicity, providing a convenient alternative to labor-intensive micro-fabrication methods for making metal-molecule-metal junctions (Fig. 2). Unlike STM, in CS-AFM the probe is positioned using normal force feedback, which decouples the probe positioning from the sample conductivity [19]. Hence, the surface topography of the film and its electrical conductivity can be acquired simultaneously and independently. Thus, CS-AFM is a promising approach for studying electron transport through molecular junctions [20].

In addition to the conductivity measurements, we carried out phase imaging in tapping mode using supersharp probes to obtain high-spatial-resolution images of the PyTp-DNA complex film on polished silicon substrate. We used supersharp silicon probes (type SSS-NCL, Nanosensors) with tip radius of 2 nm, spring constant of 47 N/m, and resonance frequency of 188 kHz. All measurements were carried out in ambient conditions at a temperature of 25 °C and relative humidity of  $\sim 30\%$ .

## III. RESULTS AND DISCUSSION

The monolayer films of PyTp and PyTp-DNA complexes were transferred to substrates at a target surface pressure of 35 mN/m by the LB technique. At this surface pressure, the molecules arrange themselves in an edge-on configuration [5]. Most of the studies of lipid-DNA complexes are aimed at

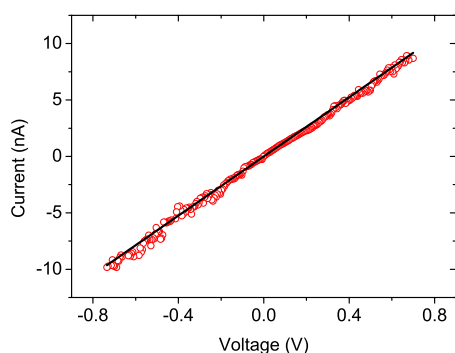


FIG. 3. (Color online) Current ( $I$ ) versus voltage ( $V$ ) characteristics measured for a gold-coated mica substrate at a constant force of 4 nN. The solid line represents a straight line fit to the experimental data points (open circles). The slope yields a value of nearly 100 M $\Omega$  for the contact resistance.

revealing supramolecular structures for nonviral gene delivery [21]. There are some efforts for using such systems in organic electronics. Okahata *et al.* have reported anisotropic electric conductivity in aligned DNA-surfactant complex films [22]. However, no nanoscale electrical conductivity measurements using CS-AFM have previously been reported on such films.

Prior to performing the current imaging and  $I$ - $V$  measurements on PyTp and PyTp-DNA complex LB films, we tested the conductivity of the AFM tip by performing  $I$ - $V$  spectroscopy with a platinum-coated tip in contact with a bare gold film coated on mica. Figure 3 shows the  $I$ - $V$  characteristics measured on a bare gold surface at a constant force of 4 nN. The measured  $I$ - $V$  curve was a straight line whose slope yielded a value of nearly 100 M $\Omega$  for the contact resistance. This might be due to a thin layer of moisture on the surface of the substrate, which is likely since the measurement was carried out in ambient conditions. In addition, the contact resistance depends on the contact force between the tip and sample. The contact resistance can decrease by several orders of magnitude by increasing the contact force. But increasing the contact force may damage the film. Therefore, we have selected the contact force carefully such that there was no film damage, and at the same time, we could get appreciable amount of current.

#### A. Current Images

The PyTp monolayer film was deposited on a gold-coated mica substrate by the LB technique and was imaged by contact-mode CS-AFM. By maintaining a constant force of 4 nN between the tip and sample, simultaneous topographic and current images were obtained for sample bias voltages of 0.1, 1, and 2 V. At a sample bias of 0.1 V, there was negligible current. This was within the error bar and hence not measurable. For the sample bias voltage of 1 V, a current flow in the range of 0.1–0.4 nA was observed. The current features were further resolved by increasing the sample bias to 2 V. The simultaneously acquired topography and current images for pure PyTp monolayer film at a bias voltage of 2 V are shown in Figs. 4(a) and 4(b), respectively. At this

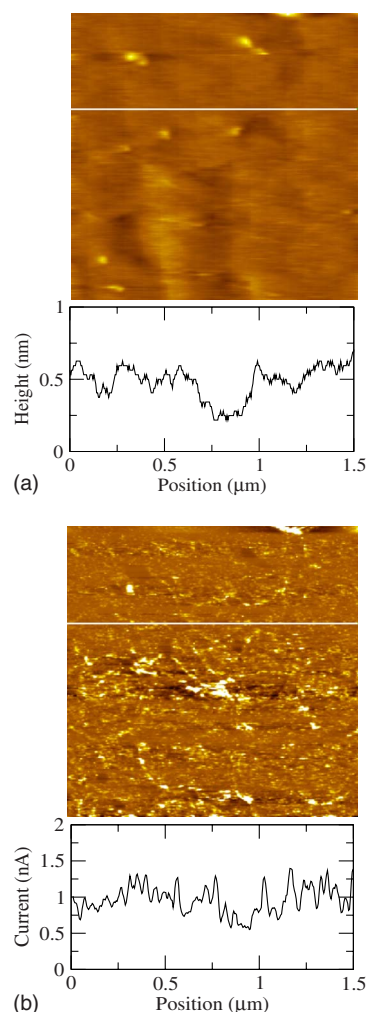


FIG. 4. (Color online) CS-AFM images for PyTp monolayer film on a gold-coated mica substrate at a sample bias of 2 V and a constant force of 4 nN: (a) topography showing the surface roughness and (b) current image showing an average current of about 1 nA across the film.

bias voltage, a current flow of about 1 nA was observed across the film. The inhomogeneities observed in the current image might be due to the defects in the gold coating on the mica substrate. Similar inhomogeneities were also observed for bare gold film coated on mica. Further, the probe works in contact mode in our methodology. The effects of contact forces are slight compression of the film and changes in the contact area itself due to the film surface roughness. These are also possible reasons for current inhomogeneities. Such inhomogeneities in current images are also reported in the literature for organic films [11,14]. The PyTp-DNA complex monolayer film formed on a gold-coated mica substrate was also imaged by CS-AFM. The PyTp-DNA complex film exhibited appreciable conductivity only above 1 V sample bias.

In addition, we prepared films on polished doped silicon substrates. The polished silicon substrate, being atomically flat, elucidates the actual topographical variation in the film surface, whereas, on a gold surface which is rough compared to a polished silicon surface, such variations are difficult to observe. The rms value of the roughness for bare silicon

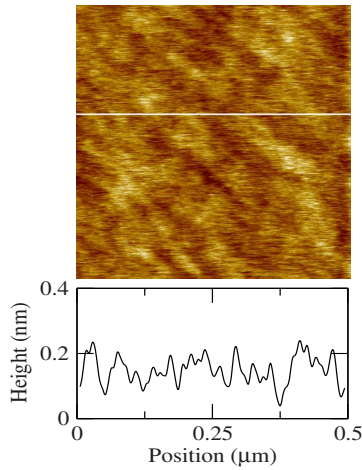


FIG. 5. (Color online) Topography image of a clean silicon substrate showing a flat surface with rms roughness of 0.06 nm.

substrate was 0.06 nm (Fig. 5). The pure PyTp film on silicon substrate showed a smooth film surface with a rms value of roughness of  $\sim 0.2$  nm [18]. Phase imaging in tapping mode was performed with supersharp probes with a tip radius  $\sim 2$  nm on the PyTp-DNA complex film in order to get a high-spatial-resolution image of the surface. Phase imaging is known to improve the resolution and contrast as compared with the topography image [23]. Figures 6(a) and 6(b) show the topography and phase images of the monolayer film of PyTp-DNA complex, respectively, on a polished doped silicon substrate. The height and phase shift profiles for the lines drawn on the corresponding images are shown in Fig. 6(c). The topography revealed a compact film surface. The phase image revealed a periodic structure which was not resolved clearly in the topography image. The Fourier transform of the phase image [shown as an inset in Fig. 6(b)] indicated a twofold symmetry. The autocorrelation of the phase image gave a periodicity of 36 nm for the complex film surface. This value is much greater than the diameter of a DNA double strand ( $\sim 2$  nm), suggesting these to be DNA bundles. The strong  $\pi$ - $\pi$  stacking interaction between the cores of the disk-shaped PyTp molecules brings multiple DNA strands together, forming bundles. Additionally, the alignment of these DNA bundles in the periodic structure was observed predominantly in the film deposition direction. In the literature, this has been attributed to the possibility that when a substrate is withdrawn from the subphase in the process of LB film deposition, the receding meniscus force tries to align the DNA strands parallel to its direction [24,25].

Next, we carried out current imaging on the same film in contact mode by maintaining a constant force of 6 nN. Figures 7(a) and 7(b) show the simultaneously acquired topography and current images for the complex monolayer film on doped silicon substrate at a sample bias of  $-7$  V. We would like to mention that due to the presence of a native oxide layer on silicon substrates, the voltage required for current imaging was high. Such high voltages are also reported in the literature for silicon with an oxide layer [26]. Figure 7(c) shows the height and current profiles corresponding to the lines drawn on the respective images. We show the profiles for three different positions on the film for better clarity. For

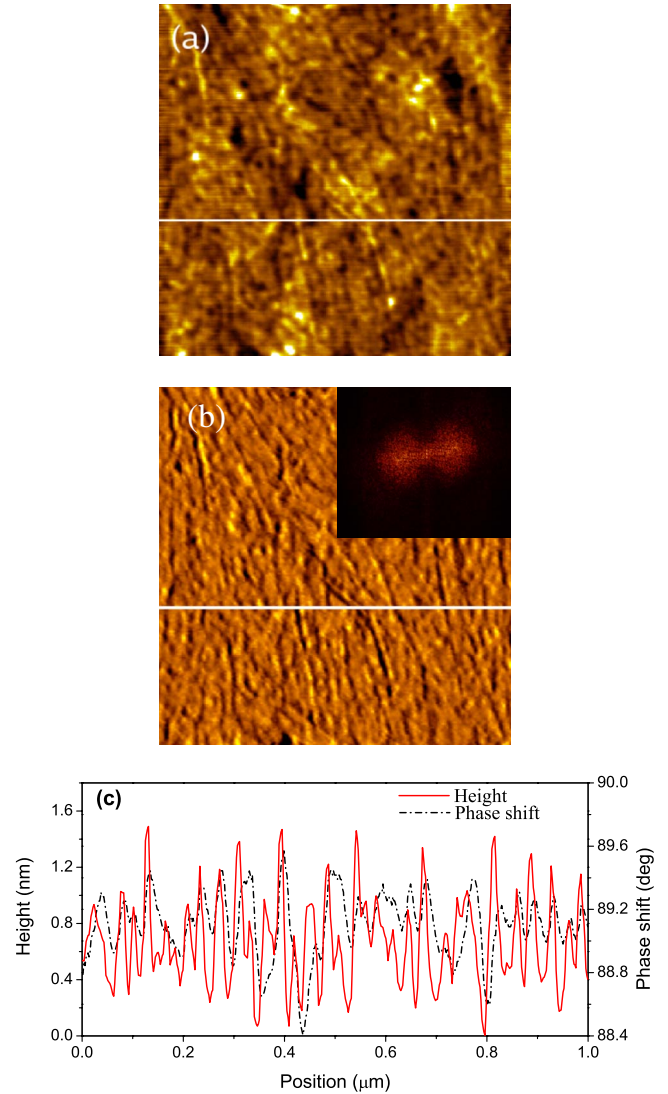


FIG. 6. (Color online) Tapping-mode AFM image of PyTp-DNA complex monolayer film on a silicon substrate: (a) Topography image. (b) Simultaneously acquired phase image. Inset shows the Fourier transform of the image. Autocorrelation of this image yields a periodicity of about 36 nm. (c) The height and phase shift profiles corresponding to the lines drawn on the topography and phase images.

current imaging, we used conducting probes with a tip radius of  $\sim 30$  nm. It is known that the spatial resolution of measurements is limited by the end radius of the probe. Hence, the current-sensing AFM tip (radius  $\sim 30$  nm) senses the periodic variation on the surface of the complex film as seen in Fig. 7(c), but not as clearly as it was sensed by the supersharp tip with radius of  $\sim 2$  nm. Therefore, the minimum height sensed by the CS-AFM tip does not correspond to the actual depth where there is no DNA on the periodic surface. However, the variation in conductivity revealed in the current image [Fig. 7(b)] may be attributed directly to the topographical variations in the film surface itself since the probe works in contact mode. Thus, we have tried to find a correspondence between the topography and current profiles [Fig. 7(c)]. We find that the current values were about 0.004 nA at

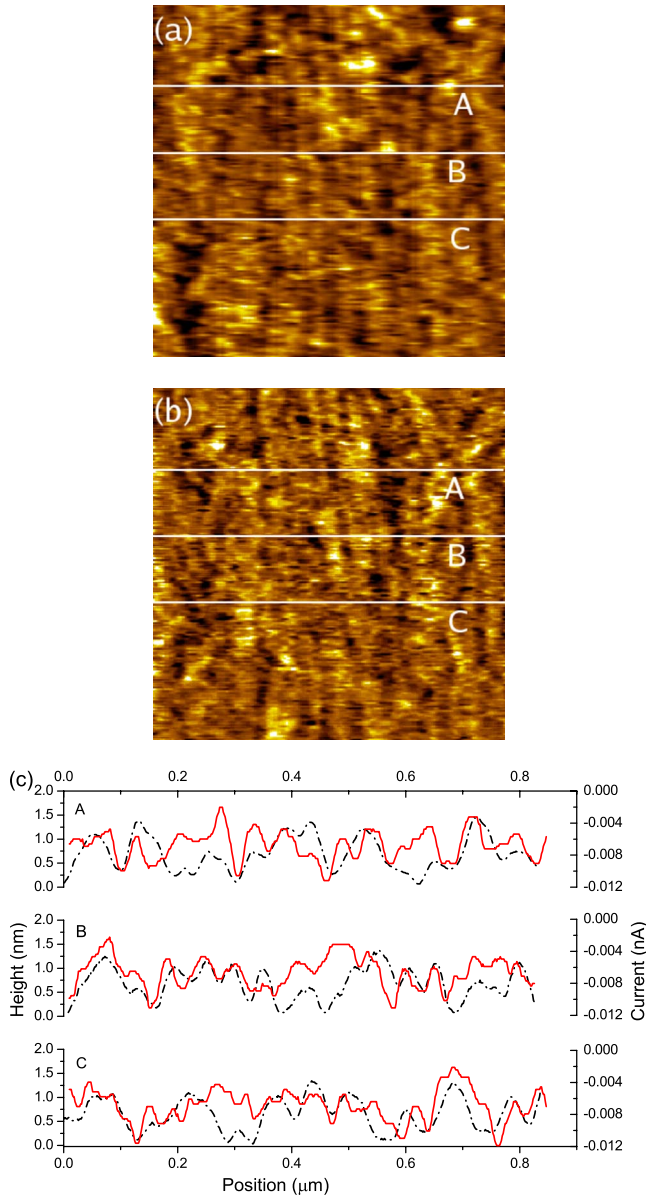


FIG. 7. (Color online) CS-AFM images for PyTp-DNA complex monolayer film on a silicon substrate with a constant force of 6 nN and a sample bias of  $-7$  V: (a) Topography image. (b) Current image. (c) The height (dash-dotted line) and current (solid line) profiles corresponding to the lines drawn at three different positions on the respective topographic and current images. The current values are represented in negative scale in order to emphasize the anticorrelation between the magnitude of the current and the height of the film.

positions where the film thickness was high, whereas they were about  $0.01$  nA at positions where the film thickness was low. We have represented the current values in Fig. 7(c) in the negative scale in order to emphasize the anticorrelation between the magnitude of the current and the height of the film. In addition, after performing current imaging in contact mode, we again scanned the same region of the film in tapping mode and we found no damage to the film.

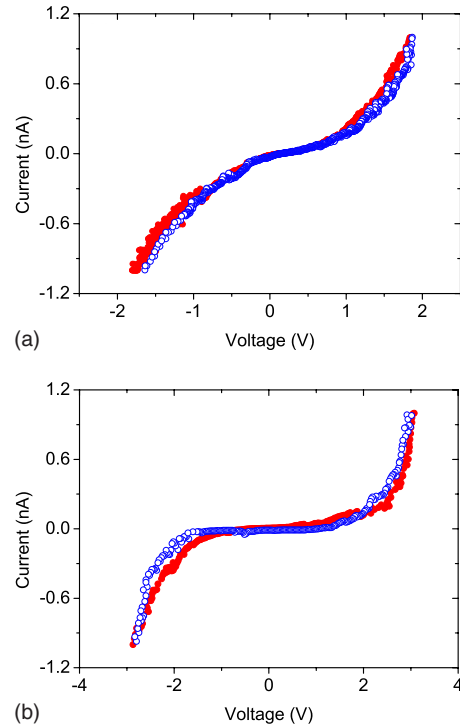


FIG. 8. (Color online) Typical  $I$ - $V$  characteristics measured by CS-AFM on monolayer films of (a) PyTp and (b) PyTp-DNA complex, on gold-coated mica substrates at a constant force of 4 nN. The solid circles represent a forward voltage scan, and the open circles represent a reverse voltage scan.

### B. $I$ - $V$ spectroscopy

The  $I$ - $V$  measurements were performed at various positions on both the pure and complex films formed on gold-coated mica substrates. The  $I$ - $V$  curves were acquired while the tip was held at a fixed position with a constant force of 4 nN and the applied voltage ramp was from  $-3$  to  $+3$  V with a scan rate of 1 Hz. The metal substrate, the film, and the conducting tip form a nanoscopic metal-insulator-metal ( $M$ - $I$ - $M$ ) junction. Representative  $I$ - $V$  curves on pure film and complex film are shown in Figs. 8(a) and 8(b), respectively. In both the cases, forward and reverse currents are found to offset by a small value ( $10$ – $14$  pA) from the zero-current line due to the charging current of the system capacitance [27]. The tunneling current rapidly increased above a certain threshold voltage for both films. For a given applied voltage, the value of current for PyTp film was significantly larger than that for PyTp-DNA complex film. With an applied bias of 1 V, the average electrical currents through PyTp and PyTp-DNA complex films were 0.2 nA and 0.05 nA, respectively.

The shape of the  $I$ - $V$  curves strongly suggests a barrier for electron transport at the tip-sample interface. The barrier height at the interface is an important parameter for electron transfer across the interface. One can choose an appropriate model to describe the measured  $I$ - $V$  curves and to determine the barrier height between the film and the metal substrate. We have considered two basic mechanisms for electron transport across a potential barrier: thermionic emission

(Schottky emission) and electron tunneling. Thermionic emission can occur when the electrons have enough energy to pass over the potential barrier. When electrons do not have sufficient energy, tunneling is the main mechanism for electron transport. In the thermionic emission model for a  $M$ - $I$ - $M$  junction, the derivative  $dI/dV$  decreases with increasing current [28]. In contrast,  $dI/dV$  increases with increasing current in the measured  $I$ - $V$  curves. Therefore, the nature of the  $I$ - $V$  curves suggests that electron tunneling is the possible mechanism for electron transport in our system. For interpreting electron tunneling, the Fowler-Nordheim (FN) model is widely used [29,30]. This model describes the electron tunneling from a metal's Fermi level over a barrier into an adjacent material. For a  $M$ - $I$ - $M$  structure, the FN tunneling current is given by the equation [31,32]

$$I = \frac{A_{eff} q^3 E^2 m}{8 \pi h \Phi_b m^*} \exp \left[ \frac{-8 \pi \sqrt{2 m^*} \Phi_b^{3/2}}{3 h q E} \right], \quad (1)$$

where  $A_{eff}$  is the effective contact area,  $E$  is the applied electric field,  $\Phi_b$  is the contact barrier height, and  $q$ ,  $m^*$ ,  $m$ , and  $h$  are electron charge, effective mass of the electron, free electron mass, and Plank constant, respectively. If we assume  $E = V/d$ , where  $V$  is the applied voltage and  $d$  is the separation between the two electrodes, then

$$I = A V^2 \exp(-B/V), \quad (2)$$

where

$$A = \frac{A_{eff} q^3 m}{8 \pi h \Phi_b d^2 m^*} \quad (3)$$

and

$$B = \frac{8 \pi \sqrt{2 m^*} \Phi_b^{3/2} d}{3 h q} = 6.83 d \left( \frac{m^*}{m} \right)^{1/2} \Phi_b^{3/2}. \quad (4)$$

Here the units of  $B$ ,  $d$ , and  $\Phi_b$  are V, nm, and eV, respectively. In our system, the separation between the two electrodes ( $d$ ) is the distance between the probe and the gold substrate. Since the tip of the probe is located just at the surface of the LB film,  $d$  is same as the thickness of the film [30]. The interpretation of  $I$ - $V$  characteristics in CS-AFM is straightforward as compared to STM studies due to the absence of an additional tunneling gap between the probe and sample surface.

Figures 9(a) and 10(a) show the log-linear representation of typical  $I$ - $V$  characteristics for the pure and complex films, respectively. In recent reports by Casuso *et al.* [29] and Beebe *et al.* [33], a transition from direct tunneling to injection tunneling was observed. The log-linear representation of the  $I$ - $V$  curves in these two reports clearly indicated the transition between the two regimes. Further, it was highlighted by Casuso *et al.* that the presence of two different transport regimes made it possible to measure the effective mass  $m^*$  and effective area  $A_{eff}$ . In our system, we did not observe an indication of a transition in the log-linear representation of the  $I$ - $V$  characteristics. Hence, it was not possible for us to determine the effective electron mass  $m^*$  and effective contact area  $A_{eff}$ . Consequently, the  $A$  value [Eq. (3)] was not very useful in our case. We have used the  $B$  value [Eq. (4)]

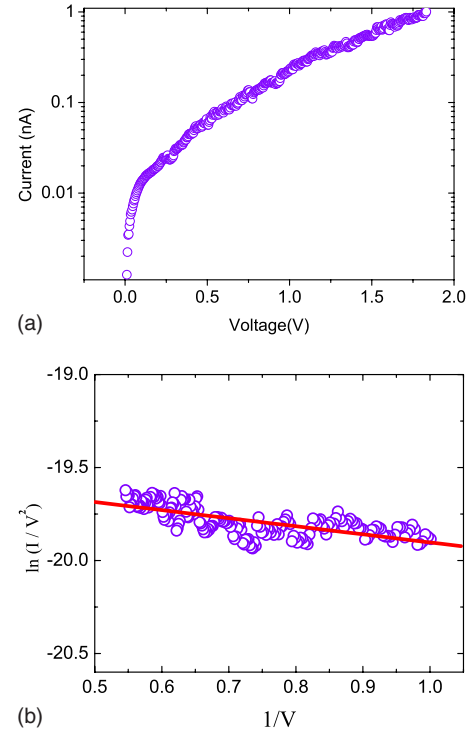


FIG. 9. (Color online) (a) Log-linear representation and (b) Fowler-Nordheim fitting to a typical  $I$ - $V$  characteristic curve measured for pure PyTp film on a gold-coated mica substrate at a constant force of 4 nN. Open circles represent the experimental data, and the solid line represents the fit.

for extracting the barrier heights for both the pure and complex films. For similar reasons, when it is difficult to calculate  $A_{eff}$ , researchers generally use the  $B$  value to extract the barrier height [28].

We have fitted the  $I$ - $V$  data for pure and complex films with the FN model [Eq. (2)]. Figures 9(b) and 10(b) show the FN plot of  $\ln(I/V^2)$  against  $1/V$  for pure and complex films, respectively. The FN plot shows a straight line whose slope yields the  $B$  value [30]. The open circles represent the experimental data points, and the solid line represents the fit. We find that the  $I$ - $V$  data of both the films fit well with this model. It is to be noted that the FN plot is an approximation in the high-voltage regime [31]. Therefore, we have shown the fitting of our data for the high-voltage regime only. At lower voltages, the system charging, thermal, and Schottky effects become dominant, which deprives us from extracting any meaningful information at that regime. To this end, sophisticated methodology such as introduced by Casuso *et al.* is essential [29]. On the basis of our analysis and within our experimental limits, we find the FN model to be a possible mechanism for electron transport in our system.

We have obtained several  $I$ - $V$  curves at different positions on the films and fitted them with the FN model. Figure 11 shows the  $B$  values obtained for 14 such  $I$ - $V$  curves measured at different positions on pure and complex films. The average  $B$  values obtained from Fig. 11 were 0.85 and 6.6 V for pure and complex films, respectively. The film thicknesses, as determined by scratching the films with an AFM tip, were 2.2 nm for PyTp and 3.2 nm for PyTp-DNA com-

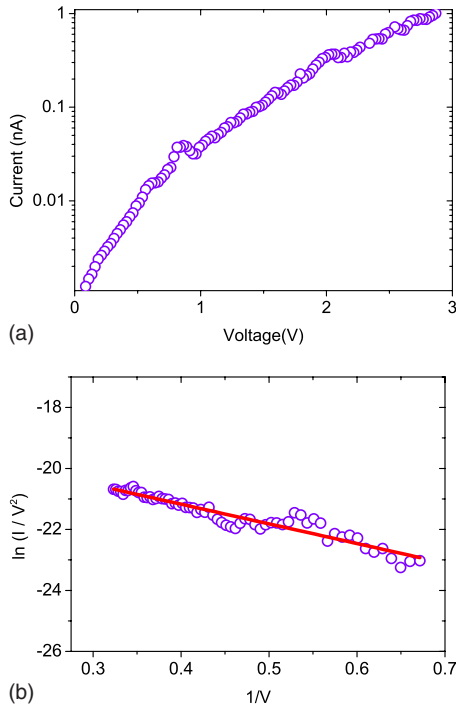


FIG. 10. (Color online) (a) Log-linear representation and (b) Fowler-Nordheim fitting to a typical  $I$ - $V$  characteristic curve measured for PyTp-DNA complex film on a gold-coated mica substrate at a constant force of 4 nN. Open circles represent the experimental data, and the solid line represents the fit.

plex. Using the average  $B$  values and the corresponding film thicknesses in Eq. (4), we have calculated the barrier heights  $\Phi_b$  to be  $0.15(m/m^*)^{1/3}$  eV and  $0.45(m/m^*)^{1/3}$  eV for pure and complex films, respectively.

In the literature, direct tunneling is known to be dominant for alkyl systems [34], due to their large highest occupied molecular orbital and lowest unoccupied molecular orbital (HOMO-LUMO) gaps ( $\sim 8$  eV). Direct tunneling refers to nonresonant tunneling (electrons tunnel directly from metal to metal) that occurs when the applied bias voltage is less than the barrier height. In contrast to the alkyl system, the mechanism of charge transport in junctions containing  $\pi$ -conjugated molecules is different. For  $\pi$ -conjugated species, the decreased HOMO-LUMO gap increases the likelihood of injection tunneling. Injection tunneling refers to resonant tunneling (electrons are injected first into the insulator and then arrive at the second electrode) which occurs in the Fowler-Nordheim regime ( $V > \Phi_b$ ). Recently, Beebe *et al.* have observed a transition from direct tunneling ( $V < \phi_b$ ) to injection tunneling ( $V > \phi_b$ ) for  $\pi$ -conjugated systems [33]. However, in our system direct tunneling may not be feasible. For disk-shaped liquid crystals, the packing and supramolecular order, which depend on their chemical structures, drastically influence the electronic properties [1]. In our system, the PyTp molecules in the LB films are arranged in columns. It appears that due to the delocalized  $\pi$ -orbital wave functions, a quasiband structure might have formed

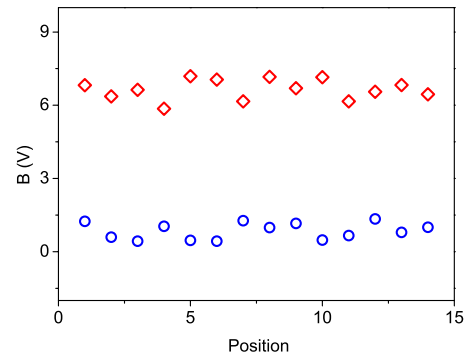


FIG. 11. (Color online) The  $B$  values obtained from the Fowler-Nordheim fitting of the  $I$ - $V$  curves measured at 14 different positions on PyTp ( $\circ$ ) and PyTp-DNA complex ( $\diamond$ ) films. The average  $B$  values are 0.85 V for the pure film and 6.6 V for the complex film.

with a very small band gap [35]. Our FN fitting results also suggest that for pure film the barrier height may be as low as 0.15 eV.

For the PyTp-DNA complex system, we find that the presence of DNA leads to a further barrier to electron transport. But it is difficult to quantify or comment on the conductivity of DNA molecules alone from such an experiment. The higher barrier height is likely to be a direct consequence of a change in packing of the molecules. The conformation of a DNA molecule and the environment in which it is present have a crucial impact on its conductivity [7]. On the basis of our observations, we find that complexation with DNA makes the film more resistive. However, a complete quantitative understanding of the type of electron transport needs detailed information about the electronic structure of the system as well as a more sensitive and sophisticated instrumental setup.

#### IV. CONCLUSIONS

We have measured the nanoscale electrical conductivity of Langmuir-Blodgett films of an ionic disk-shaped liquid crystal, PyTp and PyTp-DNA complex, by current-sensing atomic force microscopy. We find that the  $I$ - $V$  curves fit well with the Fowler-Nordheim model, indicating the electron tunneling to be a possible mechanism for electron transport. Further, analysis of the  $I$ - $V$  curves based on the FN model reveals the barrier height of PyTp-DNA complex film to be 3 times higher compared to that of pure PyTp film. Such systems can find applications as advanced materials in organic electronics.

#### ACKNOWLEDGMENTS

We would like to thank Sandeep Kumar and Santanu Kumar Pal for kindly providing us the pyridinium salt tethered with hexaalkoxytriphenylene (PyTp) material for our experiments. We thank the referees for some very useful suggestions.

- [1] S. Sergeev, W. Pisula, and Y. H. Geerts, *Chem. Soc. Rev.* **36**, 1902 (2007).
- [2] C. M. Gordon, J. D. Holbrey, A. R. Kennedy, and K. R. Seddon, *J. Mater. Chem.* **8**, 2627 (1998).
- [3] M. Yoshio, T. Mukai, H. Ohno, and T. Kato, *J. Am. Chem. Soc.* **126**, 994 (2004).
- [4] L. Cui, J. Miao, and L. Zhu, *Macromolecules* **39**, 2536 (2006).
- [5] A. Nayak and K. A. Suresh, *J. Phys. Chem. B* **112**, 2930 (2008).
- [6] D. Porath, A. Bezryadin, S. de Vries, and C. Dekker, *Nature (London)* **403**, 635 (2000).
- [7] R. G. Endres, D. L. Cox, and R. R. P. Singh, *Rev. Mod. Phys.* **76**, 195 (2004).
- [8] D. K. Schwartz, *Surf. Sci. Rep.* **27**, 241 (1997).
- [9] G. V. Nazin, X. H. Qiu, and W. Ho, *Science* **302**, 77 (2003).
- [10] N. P. Guisinger, N. L. Yoder, and M. C. Hersam, *Proc. Natl. Acad. Sci. U.S.A.* **102**, 8838 (2005).
- [11] X. D. Cui *et al.*, *Nanotechnology* **13**, 5 (2002).
- [12] M. Freitag, M. Radosavljevic, W. Clauss, and A. T. Johnson, *Phys. Rev. B* **62**, R2307 (2000).
- [13] I. Casuso, L. Fumagalli, J. Samitier, E. Padros, L. Reggiani, V. Akimov, and G. Gomila, *Nanotechnology* **18**, 465502 (2007).
- [14] D.-H. Han, J.-W. Kim, and S.-M. Park, *J. Phys. Chem. B* **110**, 14874 (2006).
- [15] G. B. Sukhorukov, M. M. Montrel, A. I. Petrov, L. I. Shabarchina, and B. I. Sukhorukov, *Biosens. Bioelectron.* **11**, 913 (1996).
- [16] W. Pisula *et al.*, *Adv. Mater. (Weinheim, Ger.)* **17**, 684 (2005).
- [17] S. Kumar and S. K. Pal, *Tetrahedron Lett.* **46**, 4127 (2005).
- [18] A. Nayak, K. A. Suresh, S. K. Pal, and S. Kumar, *J. Phys. Chem. B* **111**, 11157 (2007).
- [19] J. Reichert, R. Ochs, D. Beckmann, H. B. Weber, M. Mayor, and H. v. Lohneysen, *Phys. Rev. Lett.* **88**, 176804 (2002).
- [20] D. J. Wold and C. D. Frisbie, *J. Am. Chem. Soc.* **122**, 2970 (2000).
- [21] D. D. Lasic and N. S. Templeton, *Adv. Drug Delivery Rev.* **20**, 221 (1996).
- [22] Y. Okahata, T. Kobayashi, K. Tanaka, and M. Shimomura, *J. Am. Chem. Soc.* **120**, 6165 (1998).
- [23] X. Chen, S. L. McGurk, M. C. Davies, C. J. Roberts, K. M. Shakesheff, S. J. B. Tendler, P. M. Williams, J. Davies, A. C. Dawkes, and A. Domb, *Macromolecules* **31**, 2278 (1998).
- [24] A. Bhaumik, M. Ramakanth, L. K. Brar, A. K. Raychaudhuri, F. Rondelez, and D. Chatterji, *Langmuir* **20**, 5891 (2004).
- [25] Y. Okahata, T. Kobayashi, and K. Tanaka, *Langmuir* **12**, 1326 (1996).
- [26] A. Olbrich, B. Ebersberger, and C. Boit, *Appl. Phys. Lett.* **73**, 3114 (1998).
- [27] P. Mishra, P. Karmakar, and D. Ghose, *Nucl. Instrum. Methods Phys. Res. B* **243**, 16 (2006).
- [28] D. Xu, G. D. Watt, J. N. Harb, and R. C. Davis, *Nano Lett.* **5**, 571 (2005).
- [29] I. Casuso, L. Fumagalli, J. Samitier, E. Padros, L. Reggiani, V. Akimov, and G. Gomila, *Phys. Rev. E* **76**, 041919 (2007).
- [30] K. Yano *et al.*, *Appl. Phys. Lett.* **68**, 188 (1996).
- [31] J. G. Simmons, *J. Appl. Phys.* **34**, 1793 (1963).
- [32] M. Lenzlinger and E. H. Snow, *J. Appl. Phys.* **40**, 278 (1969).
- [33] J. M. Beebe, B. S. Kim, J. W. Gadzuk, C. D. Frisbie, and J. G. Kushmerick, *Phys. Rev. Lett.* **97**, 026801 (2006).
- [34] W. Wang, T. Lee, and M. A. Reed, *Phys. Rev. B* **68**, 035416 (2003).
- [35] X. Crispin *et al.*, *J. Am. Chem. Soc.* **126**, 11889 (2004).